Heliyon 10 (2024) e28914

Contents lists available at ScienceDirect

Heliyon

journal homepage: www.cell.com/heliyon

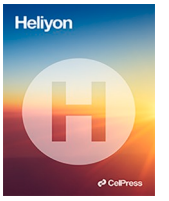

Research article

Low-dose CT fluoroscopy–guided interventional minimally invasive robot

Xiaofeng He, Yueyong Xiao *, Xiao Zhang, Xiaobo Zhang, Xin Zhang, Yingtian Wei, Zhongliang Zhang, Xiaodong Xue, Shiwen Zhang

The First Medical Center of Chinese PLA General Hospital, Department of Diagnostic Radiology, Beijing, China

ARTICLE INFO

Keywords:
CT fluoroscopy
Low-dose
Robot-assisted
Teleoperation

ABSTRACT

Background: This study aimed to assess the feasibility, safety, and accuracy of a low-dose CT fluoroscopy-guided remote-controlled robotic real-time puncture procedure.
Methods: The study involved two control groups with Taguchi method: Group A, which underwent low-dose traditional CT-guided manual puncture (blank control), and Group B, which underwent conditional control puncture. Additionally, an experimental group, Group C, underwent CT fluoroscopy-guided remote-controlled robotic real-time puncture. In a phantom experiment, various simulated targets were punctured, while in an animal experiment, attempts were made to puncture targets in different organs of four pigs. The number of needle adjustments, puncture time, total puncture operation time, and radiation dose were analyzed to evaluate the robot system.
Results: Successful punctures were achieved for each target, and no complications were observed. Dates were calculated for all parameters using Taguchi method.
Conclusion: The low-dose CT fluoroscopy-guided puncture robot system is a safe, feasible, and equally accurate alternative to traditional manual puncture procedures.

1. Introduction

Traditional computed tomography (CT)-guided interventions involve manual puncture procedures, where doctors rely on their experience to handle the needles based on intermittent CT scans. However, this approach is limited by the inability to directly visualize the needles or probes during the puncture process, leading to what is known as “blind puncture” [1,2]. To address this limitation, a CT fluoroscopy minimally invasive robot system was developed to provide real-time CT image guidance. While the traditional fluoroscopy method exposes doctors and patients to high levels of radiation, the robot system operates in a low-dose fluoroscopy mode [3–8]. This mode employs reduced radiation scanning parameters and the “click trample and view” compartment fluoroscopy technique to minimize radiation exposure. In this study, we conducted phantom and animal experiments using real-time CT fluoroscopy images to evaluate the feasibility, safety, and accuracy of robotic remote real-time puncture under low-dose CT fluoroscopy, comparing the results with those obtained from traditional CT-guided manual puncture procedures.

* Corresponding author. The First Medical Center of Chinese PLA General Hospital, Department of Diagnostic Radiology, Beijing, China.
E-mail address: xiaoyueyong@gmail.com (Y. Xiao).

https://doi.org/10.1016/j.heliyon.2024.e28914
Received 6 February 2023; Received in revised form 27 February 2024; Accepted 26 March 2024
Available online 30 March 2024

2. Materials and methods

Ethical approval for the animal experiments was obtained from the institutional animal care and use committee of our institution, with the approval number 2020-X16-43.

2.1. Robotic system

The robotic system was developed based on the UR (Universal Robots) system from the Danish Universal Robots Company in Denmark. It consisted of several components, including a control host, a remote control console, a speed control panel, a manipulator, a needle holder, a lifting base, a laser locator, a robot monitoring system, and a pedal. The configuration of the robot system in the operating room can be seen in Figs. 1 and 2.

The control host was responsible for software programming and debugging of the robot system, controlling its overall operation. Two remote control consoles were utilized, with the proximal movable console used to control the movement of the mechanical arm near the CT bed, and the distal console employed for remote needle insertion during fluoroscopy.

The mechanical arm, manufactured by the Danish Universal Robots Company, was equipped with six degrees of freedom and its movement speed could be adjusted using the speed control panel. To prevent CT artifacts caused by the metallic components of the mechanical arm and motor, the “L" needle-holding structure was employed. The needle-holding arm was crafted from materials with high transmittance, and the front-end fixing clip of the needle holder was produced using three-dimensional printing techniques (Fig. 3).

2.2. Traditional manual puncture and robotic puncture

The experimental model was positioned within the large-aperture CT scanning bore with perspective functionality for conventional CT scanning. The target to be punctured was identified and recorded. Existing literature on experimental design methods for radiation doses and various puncture techniques was consulted to optimize the experimental design [4,9–12]. Comparative studies were then conducted involving different radiation doses, manual puncture, and robot-guided puncture. Punctures were carried out using a 17G needle in both phantom and animal experiments. The radiation dose was calculated using the dose-length product, with the unit being mGy.

(1) Traditional manual puncture: Experienced interventional doctor (attending doctor with over 10 years of working experience) performed needle insertions under low-dose CT guidance. There were two groups: blank control group A (FOV: 350 mm × 350

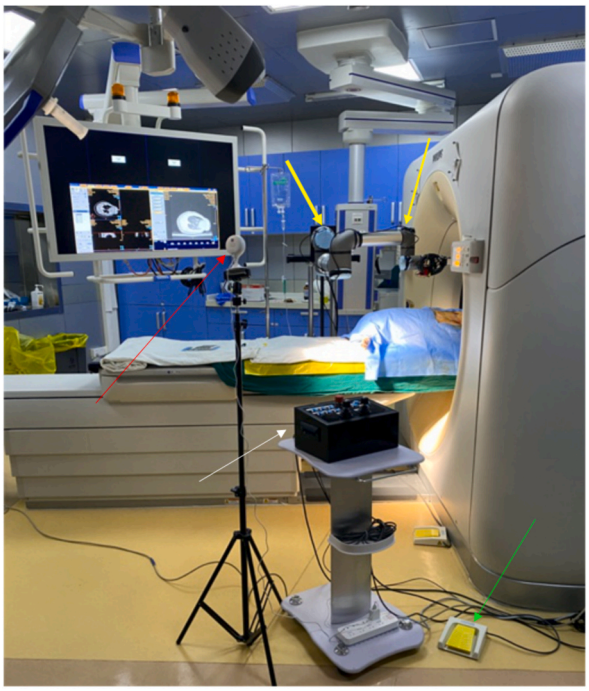

Fig. 1. Layout of the robot near the CT bed: robot manipulator (yellow arrow), movable remote control console (white arrow), monitoring camera of the robot system (red arrow), and pedal (green arrow). (For interpretation of the references to colour in this figure legend, the reader is referred to the Web version of this article.)

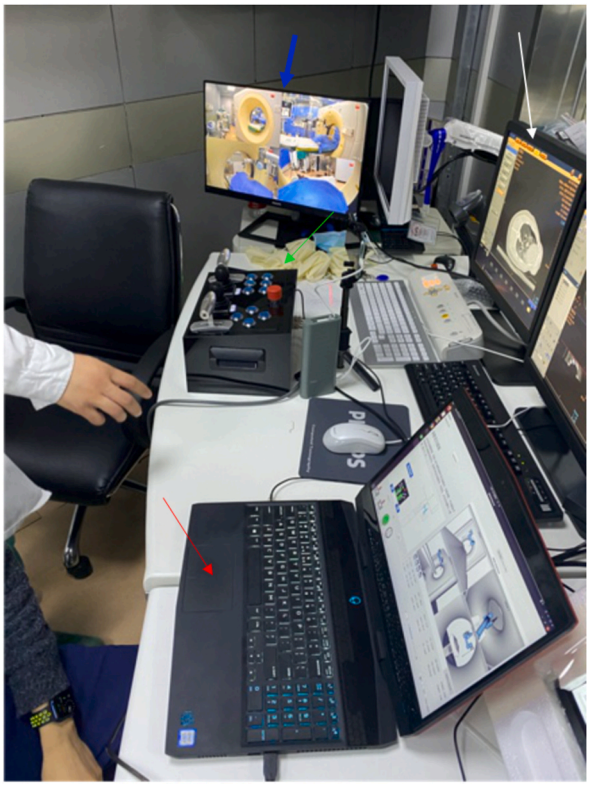

Fig. 2. Layout of the remote control compartment: remote-controlled console (green arrow), the red button on the console is the emergency stop button; monitor of CT (white arrow), robot monitoring system (blue arrow), and control host of the robot (red arrow). (For interpretation of the references to colour in this figure legend, the reader is referred to the Web version of this article.)

mm; voltage: 120 kV; current: 50 mAs; layer thickness: 5 mm) and conditional control group B (FOV: 350 mm × 350 mm; voltage: 120 kV; current: 30 mAs; layer thickness: 5 mm). The scanning range along the Z-axis was 4 cm. For the liver model, the target location was identified, and an appropriate puncture path was selected. Punctures were performed 10 times in each group. In the animal experiment, four preset metal targets (2 mm long) were placed in the upper lobe and lower lobe of the right lung and liver of the experimental pigs. The appropriate puncture path was chosen, and punctures were performed 32 times in each group.

(2) Phantom experiment of CT fluoroscopy–guided remote control robotic puncture: The scanning table was positioned according to the recorded target location. The fluoroscopy scanning parameters for experimental group C were as follows: FOV: 350 × 350 mm^2; voltage: 120 kV; current: 30 mAs; collimator width: 6 mm. The effective radiation dose was 66% of the routine radiation dose in the fluoroscopy mode. The "click trample and view" mode was employed for fluoroscopy in the CT control room. The needle entry direction was adjusted in real-time by observing the position relationship between the puncture needle tip and the target. Once the needle tip "aiming line" aligned with the target's center, the pedal was continuously pressed for low-dose fluoroscopy during the puncture, enabling real-time display of the spatial position relationship between the needle tip and the target. The "aiming line" (Fig. 4), represented by the low-density metal artifact of the puncture needle tip, remained aligned with the target as the needle holder was slowly and continuously controlled using the joystick. If the "aiming line" deviated from the target's center, slight adjustments to the joystick allowed for tuning the puncture direction. Target punctures were performed 10 times.

(3) Animal experiment of the remote-controlled robotic puncture of CT fluoroscopy: The scanning parameters used in the phantom experiment were also applied in this phase. The needle position was aligned with the scanning level based on the laser light projected onto the CT frame. In the CT control room, the position relationship between the puncture needle tip and the target point was observed using the "click trample and view" method. The doctor operated the joystick on the console to adjust the needle's position and direction. Once the extension line of the "aiming line" at the needle's front end passed through the target, the mechanical arm was lifted away from the experimental pig's body surface in the opposite direction of the needle. The doctor then entered the CT operation room and activated the laser light at the mechanical arm's front end. The intersection of the two lasers indicated the puncture point. After making a 2-mm incision on the pig's skin, the doctor carefully guided the mechanical arm towards the puncture site. In the CT control room, the "aiming line" of the puncture needle tip and the target's center were aligned in a straight line using the "click trample and view" method. Continuous low-dose fluoroscopy scanning provided real-time visualization of the spatial position of the needle tip and the target. The operator used the joystick to slowly and

Fig. 3. Connection between the mechanical arm and the needle holder: mechanical arm (yellow arrow), clamping arm of the radiopaque needle holder (red arrow), rear needle holder (black arrow) for entering the needle, front needle holder (white arrow) for avoiding the bending of the puncture needle, and one of the laser beam modules (green arrow). (For interpretation of the references to colour in this figure legend, the reader is referred to the Web version of this article.)

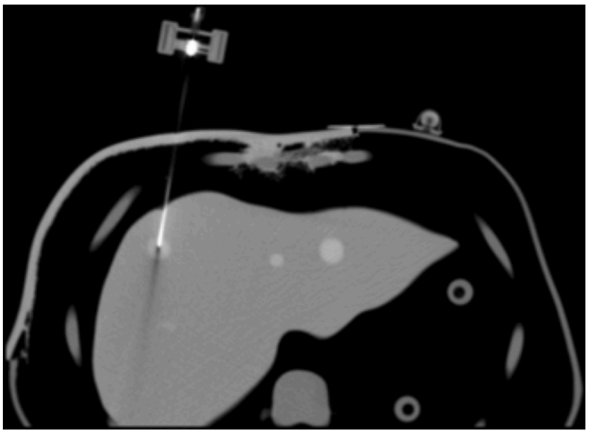

Fig. 4. In the CT fluoroscopy mode, the needle tip was punctured to the center of the target point, and the “aiming line " at the front of the needle tip could be observed.

continuously insert the needle, making adjustments as needed if the “aiming line” deviated from the target’s center. The robot monitoring system, operating in continuous fluoroscopy mode, not only displayed the puncture needle’s trajectory from various angles but also showed the ongoing puncture in real-time on the CT fluoroscopy image (Figs. 5 and 6). This enabled

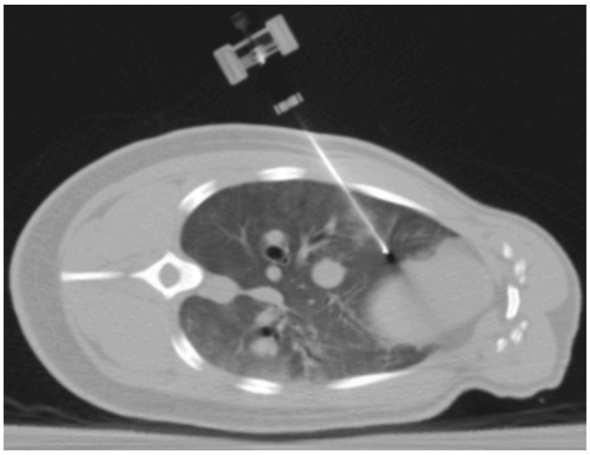

Fig. 5. Needle punctured the target in the lower lobe of the right lung accurately.

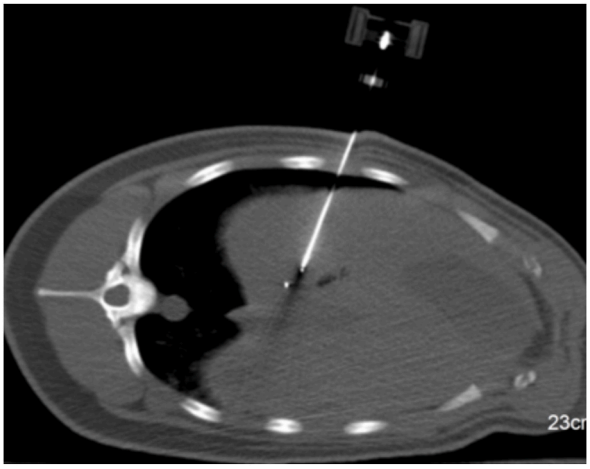

Fig. 6. Needle accurately punctured one of the metal targets in the liver.

comprehensive and real-time monitoring of the needle's position both in vitro and in vivo. A total of 16 target punctures were performed.

Experimental process with Taguchi method (Figs. 7 and 8).

After successfully reaching the target, the number of needle adjustments (N), puncture time (PT), total time (T), radiation dose (D), and precision of puncturing the target's center (P) were recorded. In the animal experiments, any complications such as pneumothorax and bleeding were noted upon needle extraction.

3. Results

A total of 30 punctures were successfully performed across the three groups. The phantom experiments were completed successfully in all groups, with a puncture accuracy of 100%. Group B exhibited a lower radiation dose compared to Group A, which was statistically significant ($P < 0.05$). However, the remaining indices did not show any statistical significance ($P > 0.05$, Table 1). Therefore, we adopted the same radiation conditions as Group B for the control group (Group C). Group C demonstrated shorter operation time, a reduced number of needle adjustments, lower puncture time (PT), and higher precision from the target's center compared to Group B ($P < 0.05$, Table 2).

Taguchi Method is a statistical test method, by selecting the appropriate orthogonal design table to arrange the trial, and then the signal-to-noise analysis and variance analysis to determine the optimal conditions of each factor and the degree of significance. Table 5 shows the factors examined and their corresponding levels.

A total of 48 punctures were successfully completed across the three groups. Among the experimental pigs, one experienced minor chest bleeding, and another had a small amount of pneumothorax following the manual puncture of the lower lobe of the right lung.

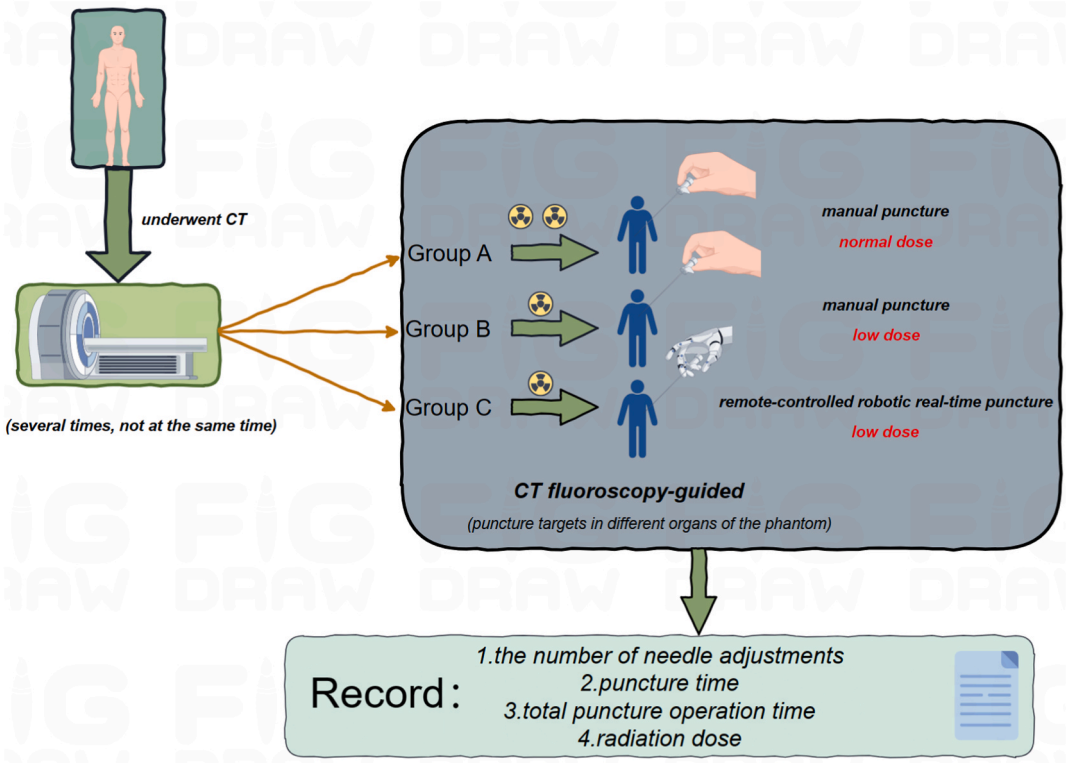

Fig. 7. Photograph of process diagram of phantom experiment.

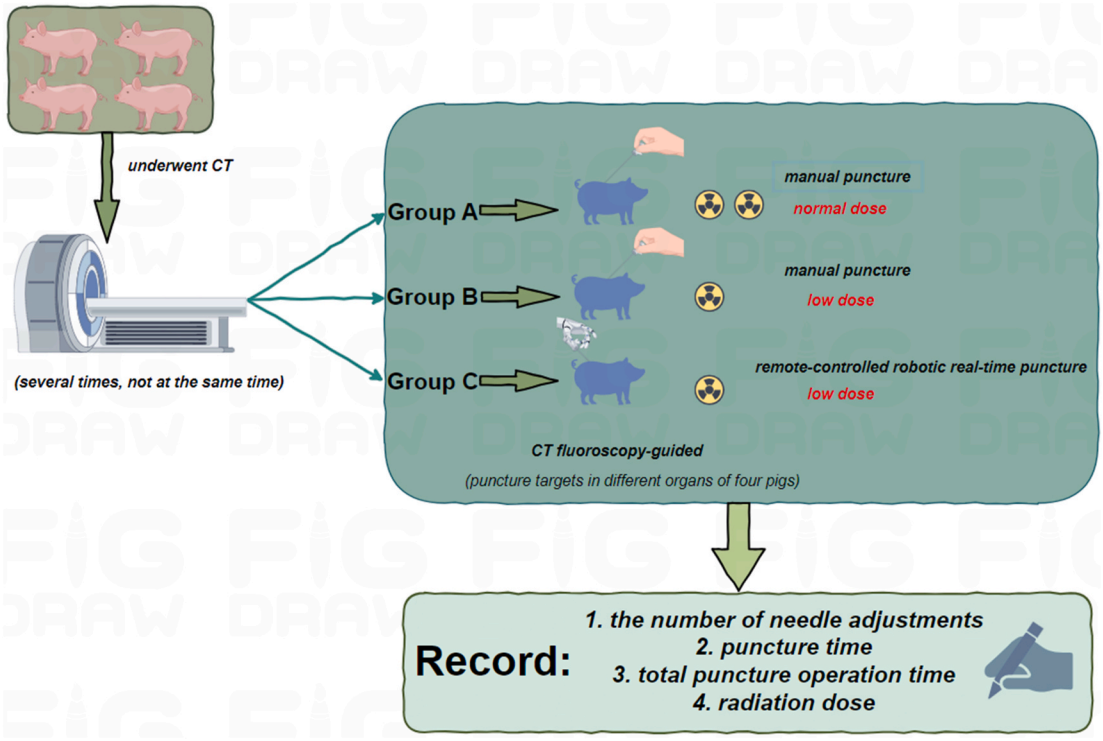

Fig. 8. Photograph of process diagram of animal experiment.

Table 1

Comparison of phantom experimental parameters in Group A and B ($\bar{x} \pm s$).

Groups	*T* (s)	*N*	PT (s)	*D* (mGy)	*P* (mm)
Group A	455.00 ± 16.53	3.80 ± 0.25	333.50 ± 15.36	99.84 ± 5.97	1.30 ± 0.15
Group B	454.00 ± 16.96	3.90 ± 0.23	335.50 ± 16.40	60.06 ± 3.59	1.40 ± 0.16
P value	> 0.05	> 0.05	> 0.05	< 0.05	> 0.05

Note:total time (T), number of needle adjustment (N), puncture time (PT), radiation dose (D), precision of puncturing the target's center(P).

Table 2

Comparison of phantom experimental parameters in Group B and C ($\bar{x} \pm s$)

Groups	*T* (s)	*N*	PT (s)	*D* (mGy)	*P* (mm)
Group B	454.00 ± 16.96	3.90 ± 0.23	335.50 ± 16.40	60.06 ± 3.59	1.40 ± 0.12
Group C	142.30 ± 2.56	1	14.90 ± 0.75*#	61.84 ± 2.82	1.20 ± 0.13
P value	< 0.05	< 0.05	< 0.05	> 0.05	> 0.05

Note:total time (T), number of needle adjustment (N), puncture time (PT), radiation dose (D), precision of puncturing the target's center(P).

Table 3

Comparison of animal experiment parameters in Group A and B ($\bar{x} \pm s$)

Groups	*T* (s)	*N*	PT (s)	*D* (mGy)
Group A	692.18 ± 38.64	5.13 ± 0.25	478.75 ± 29.65	131.24 ± 6.54
Group B	673.75 ± 36.2	5.25 ± 0.28	470 ± 25.88	82.7 ± 4.4
P value	> 0.05	> 0.05	> 0.05	< 0.05

Note:total time (T), number of needle adjustment (N), puncture time (PT), radiation dose (D).

Table 4

Comparison of animal experiment parameters in Group B and C ($\bar{x} \pm s$)

Groups	*T* (s)	*N*	PT (s)	*D* (mGy)
Group B	673.75 ± 36.2	5.25 ± 0.28	470 ± 25.88	82.7 ± 4.4
Group C	150.75 ± 3.14	1	23.25 ± 0.64	91.93 ± 2.57
P value	< 0.05	< 0.05	< 0.05	> 0.05

Note:total time (T), number of needle adjustment (N), puncture time (PT), radiation dose (D).

Table 5

Orthogonal arrays and experimental results.

Factors and levels						
	deviation	A	B	C	Dose ratio/%	S/N ratin'/dB
1	1	1	1	1	100	−47.01
2	1	2	2	2	100	−48.30
3	1	3	3	3	90	−45.85
4	2	1	2	3	80	−50.50
5	2	2	3	1	70	−46.61
6	2	3	1	2	60	−45.93
7	3	1	3	2	50	−45.06

Note:Signal-to-Noise ：S/N.

However, these occurrences did not affect the puncture procedure. The puncture accuracy in all three groups was 100%. Group B demonstrated a lower radiation dose compared to Group A, which was statistically significant ($P < 0.05$). However, the remaining indices did not show any statistical significance ($P > 0.05$, Table 3). Consequently, we selected the same radiation conditions as Group B for the control group (Group C). Group C exhibited shorter operation time, reduced needle adjustment time, and shorter puncture time (PT) compared to Group B ($P < 0.05$, Table 4).

The corresponding signal-to-noise ratio (S/N) values obtained for the three groups of tests are shown in the last two columns of Table 6. Due to the orthogonal properties of Taguchi tests, the influence of other factors can be excluded by the arithmetic averaging

Table 6
S/N response table.

Factors		SN/dB		
Dose ratio 1		Dose ratio2	Dose ratio3	MAX-MIN
A	−47.52	−47.85	−47.38	0.4621
B	−47.19	−49.72	−45.84	3.887
C	−47.99	−46.43	−48.32	1.894
Total SN: 47.58 dB				

Note：Dose ratio 1：Group A，Dose ratio 2：Group B, Dose ratio 3：Group C.

method to find the average S/N values of each factor at different levels. Figure intuitively shows the trend of each factor with different levels. In the Taguchi method, the level with the largest S/N value is always the optimal level, whether the index examined is "bigger is better" or "smaller is better". Using the data the Taguchi method can predict the SNR value S/N = −44.2682.

The significance of the effect of each factor on the CT dose can be obtained by ANOVA. Table 7 presents the results of the ANOVA analysis. Because the total sum of factor A is less than the total sum of trial error, that is, the effect of A can be ignored, it is incorporated into the error to yield the total trial error. The F-test value is an important indicator of the significance of each factor, and the greater the F-test value, the more significant the effect is. In addition, the contribution degree can also be used to roughly estimate the influence significance of each factor. This follows that factor C has the most significant effect.

Overall, the CT fluoroscopy-guided remote-controlled puncture robot system, utilized in both the phantom and animal experiments, resulted in a decreased number of puncture adjustments, shorter PT and total puncture time, reduced radiation dose, and improved puncture precision, thereby ensuring consistent accuracy.

4. Discussion

Various types of navigation equipment have been developed to enhance puncture accuracy and reduce reliance on the experience of doctors. These equipment can be classified into electromagnetic, infrared, and computer-aided positioning systems based on their working principles. Currently, notable clinical applications include the ig4 system by Veran Medical Technologies (USA), the infrared navigator by Xinbo Medical Technology Co., Ltd. (China), and the Maxio system by Perfint Company (India) [2]. However, these navigation devices rely on preoperative CT scanning images to guide the puncture, which cannot account for target displacement due to physiological movement and tissue deformation. Moreover, they fail to provide real-time observation of pathological changes resulting from the movement of the puncture needle, such as bleeding and pneumothorax. In contrast, CT fluoroscopy-guided puncture enables real-time visualization of the needle entry direction and various changes occurring during the puncture, significantly enhancing accuracy and safety [5–8]. To minimize radiation exposure, scanning parameters are optimized for low-dose fluoroscopy. Additionally, a teleoperation robotic system, known as a master-slave surgical robot, is employed to reduce fluoroscopy time. In this system, the doctor remotely controls the puncture needle while observing the images, and the robot executes the desired actions in collaboration with the doctor, facilitating the completion of the surgical procedure. Real-time evaluation of the needle entry path and the spatial relationship between the needle tip and the target enables timely adjustments of the puncture needle's position and direction, thereby achieving precise punctures.

The results demonstrated that the robotic system eliminated the need for repetitive needle adjustments within the operating room. It only required a single installation of the puncture needle for remote adjustment and insertion, significantly reducing the total puncture time (PT). The remote-controlled puncture system effectively reduced the number of adjustments and improved the precision of punctures while maintaining the same level of accuracy [9–12]. Notably, targets located in dynamic regions, such as the lower lobe of the lung and the liver adjacent to the heart, exhibited significant fluctuations due to respiration and heartbeats [13,14]. During fluoroscopy, real-time observation revealed discontinuity of the target within the scanning slice. As the target entered the scanning slice, puncture could be swiftly executed, resulting in a notable enhancement in puncture accuracy.

During the CT fluoroscopy-guided remote control robot puncture procedure, tissue compression and deformation occurred when the needle punctured different organs or even the same tissue at varying depths. This led to deviations in the "aiming line." The soft and less dense nature of lung tissue, due to the presence of gas, amplified this phenomenon. Furthermore, when the needle angle was not aligned with the pleura, hindering its rapid and complete penetration, the pleura and lung tissue were compressed. Consequently, the puncture direction deviated from the target direction. This issue was particularly prominent when puncturing lung tissue, where tissue

Table 7
Analysis of variance.

Factors	quadratic sum	free degree	mean square sum	F-test	contribution/%
A	0.3376	2	0.1688		1.079
C	23.36	2	11.68	26.14	74.65
B	6.146	2	3.073	6.877	19.64
deviation	1.450	2	0.7248		4.633

Note：Factor C is most obvious.

deformation prevented swift penetration, resulting in pushing against the visceral pleura. To address this, a free adjustment mode for the needle holder was implemented. It involved retracting the puncture needle and adjusting the insertion speed when nearing the parietal pleura. This approach ensured that the needle generated sufficient impact force and greater inertia upon passing through the visceral pleura, fully penetrating it, and enabling the manipulator to closely emulate the functionality of manual puncture. The degree of tissue deformation varied based on the angle of needle insertion. When the puncture angle was less than 30° from the vertical direction, the tissue deformation-induced position deviation of the puncture needle was minimal. However, as the angle increased, tissue deformation occurred due to the needle compressing the tissue at its tip, hindering rapid tissue penetration and resulting in larger position deviations.

We chose a double-blind randomized controlled experiment design with a statistical method of comparing the means of t-tests. The experimental results conform to a normal distribution. The phantom and animal experiments provided confirmation that the radiation dose in the blank control group (50 mAs) was significantly higher compared to the experimental group (30 mAs). The conventional tube current, set at over 100 mAs, was not controlled to minimize radiation damage to the animals. Numerous studies [4,8,13,14] have demonstrated that using 30 mAs instead of 50 mAs maintains an acceptable image signal-to-noise ratio, without compromising CT-guided puncture accuracy. However, employing 20 mAs resulted in a low image signal-to-noise ratio and poor image quality. Manual puncture involved intermittent spiral scanning, with fluoroscopy utilizing single-layer scanning and a narrow collimator width of only 6 mm. Moreover, only 66% of the rays were generated, significantly reducing the scanning radiation range [15–17]. The needle direction was calibrated using the "click trample and view" mode, while the target direction was adjusted by aligning the "aiming line" generated at the front of the needle tip with the target's center. After calibrating the needle direction in the "click trample and view" mode, continuous fluoroscopy was employed to facilitate rapid needle insertion. This combined approach also reduced the radiation dose for both the model and animals.

5. Limitations

The teleoperation robot system was securely positioned near the CT scanning table, ensuring that the mechanical arm remained relatively fixed [18–22]. Consequently, it was strictly prohibited to move the scanning table during fluoroscopy-guided puncture procedures. Any movement of the table could result in the needle shifting in relation to the animal or model, potentially causing tissue or organ damage. If the target appeared on a different scanning slice, it was necessary to perform another scan to determine the appropriate slice for targeting.

In conclusion, our self-developed low-dose CT fluoroscopy teleoperation robot system has successfully achieved real-time CT-guided puncture. The phantom experiments and experiments on various animal tissues and organs have verified the safety and feasibility of this novel puncture technique, which offers comparable accuracy to conventional manual puncture but with enhanced precision provided by the robot system. Compared to traditional CT-guided puncture methods, our robot system eliminates the need for repeated entry into the CT operation room for needle adjustments, thus reducing the number of puncture adjustments and shortening the time required for needle insertion and overall procedure duration. The radiation dose received by the phantom and animals in the low-dose CT fluoroscopy mode is significantly lower than that of traditional manual puncture methods. Additionally, doctors are not exposed to radiation due to the use of remote operation.

Data sharing statement

The datasets utilized and/or analyzed during the current study are available from the corresponding author upon reasonable request.

Checklist

This study involved animal experiments; therefore, the checklist is not applicable.

Ethical

The animal experiments conducted in this study were approved by the Institutional Animal Care and Use Committee of our institution. The approval number is 2020-X16-43.

Funding

This study was supported by the National Natural Science Foundation of China (No. 81771941). The funder had no involvement in the study design, data collection and analysis, decision to publish, or preparation of the manuscript.

CRediT authorship contribution statement

Xiaofeng He: Writing – review & editing, Writing – original draft, Validation, Supervision, Software, Resources, Project administration, Methodology, Funding acquisition, Formal analysis, Data curation, Conceptualization, Investigation, Visualization. **Yueyong Xiao:** Supervision, Investigation, Funding acquisition, Conceptualization. **Xiao Zhang:** Data curation. **Xiaobo Zhang:** Formal

analysis. **Xin Zhang:** Formal analysis. **Yingtian Wei:** Formal analysis. **Zhongliang Zhang:** Formal analysis, Data curation. **Xiaodong Xue:** Data curation. **Shiwen Zhang:** Data curation.

Declaration of competing interest

The authors declare that they have no known competing financial interests or personal relationships that could have appeared to influence the work reported in this paper.

Acknowledgments

None.

References

[1] M. Anzidei, et al., Preliminary clinical experience with a dedicated interventional robotic system for CT-guided biopsies of lung lesions: a comparison with the conventional manual technique, Eur. Radiol. 25 (5) (2015) 1310–1316, https://doi.org/10.1007/s00330-014-3508-z.
[2] X.F. He, et al., Preliminary clinical application of the robot-assisted CT-guided irreversible electroporation ablation for the treatment of pancreatic head carcinoma, Int J Med Robot 16 (4) (2020) e2099, https://doi.org/10.1002/rcs.2099.
[3] H. Prosch, et al., CT fluoroscopy-guided vs. multislice CT biopsy mode-guided lung biopsies: accuracy, complications and radiation dose, Eur. J. Radiol. 81 (5) (2012) 1029–1033, https://doi.org/10.1016/j.ejrad.2011.01.064.
[4] T. Liang, et al., Ultra-low-dose CT-guided lung biopsy in clinic: radiation dose, accuracy, image quality, and complication rate, Acta Radiol. 62 (2) (2021) 198–205, https://doi.org/10.1177/0284185120917622.
[5] T.J. Dietrich, et al., Fluoroscopy-guided versus CT-guided lumbar steroid injections: comparison of radiation exposure and outcomes, Radiology 290 (3) (2019) 752–759, https://doi.org/10.1148/radiol.2018181224.
[6] J.J. Froelich, et al., Guidance of percutaneous pulmonary biopsies with real-time CT fluoroscopy, Eur. J. Radiol. 42 (1) (2002) 74–79, https://doi.org/10.1016/s0720-048x(01)00391-6.
[7] M.U.A. Khan, et al., Reduction of operator radiation exposure using a passive robotic device during fluoroscopy-guided arterial puncture: an experimental study in a swine model, European Radiology Experimental 3 (1) (2019) 20, https://doi.org/10.1186/s41747-019-0098-1.
[8] J. Hur, et al., Computed tomographic fluoroscopy-guided needle aspiration biopsy as a second biopsy technique after indeterminate transbronchial biopsy results for pulmonary lesions: comparison with second transbronchial biopsy, J. Comput. Assist. Tomogr. 34 (2) (2010) 290–295, https://doi.org/10.1097/RCT.0b013e3181bc93ef.
[9] T. Hiraki, et al., Robotic insertion of various ablation needles under computed tomography guidance: accuracy in animal experiments, Eur. J. Radiol. 105 (2018) 162–167, https://doi.org/10.1016/j.ejrad.2018.06.006.
[10] E.A. Knott, et al., Robotically-Assisted sonic therapy for renal ablation in a live porcine model: initial preclinical results, J. Vasc. Intervent. Radiol. 30 (8) (2019) 1293–1302, https://doi.org/10.1016/j.jvir.2019.01.023.
[11] K. Cleary, et al., Precision placement of instruments for minimally invasive procedures using a "needle driver" robot, Int J Med Robot 1 (2) (2005) 40–47, https://doi.org/10.1002/rcs.40.
[12] T. Hiraki, et al., Zerobot®: a remote-controlled robot for needle insertion in CT-guided interventional radiology developed at okayama university, 72 6:539-546, https://doi.org/10.18926/AMO/56370, 2018.
[13] Q.M.B. De Ruiter, et al., Endobronchial navigation guided by cone-beam CT-based augmented fluoroscopy without a bronchoscope: feasibility study in phantom and swine, J. Vasc. Intervent. Radiol. 31 (12) (2020) 2122–2131, https://doi.org/10.1016/j.jvir.2020.04.036.
[14] S.K. Carlson, et al., Intermittent-mode CT fluoroscopy-guided biopsy of the lung or upper abdomen with breath-hold monitoring and feedback: system development and feasibility, Radiology 229 (3) (2003) 906–912, https://doi.org/10.1148/radiol.2293021496.
[15] X. Han, et al., Safety and accuracy of robot-assisted versus fluoroscopy-assisted pedicle screw insertion in thoracolumbar spinal surgery: a prospective randomized controlled trial, J. Neurosurg. Spine (2019) 1–8, https://doi.org/10.3171/2018.10.SPINE18487.
[16] J.K. Hoang, et al., Radiation dose exposure for lumbar spine epidural steroid injections: a comparison of conventional fluoroscopy data and CT fluoroscopy techniques, AJR Am. J. Roentgenol. 197 (4) (2011) 778–782, https://doi.org/10.2214/ajr.10.6102.
[17] C.A. Burgard, et al., CT fluoroscopy-guided percutaneous osteoplasty with or without radiofrequency ablation in the treatment of painful extraspinal and spinal bone metastases: technical outcome and complications in 29 patients, Diagn. Interventional Radiol. 24 (3) (2018) 158–165, https://doi.org/10.5152/dir.2018.17265.
[18] S. Liu, et al., Automatic multiple-needle surgical planning of robotic-assisted microwave coagulation in large liver tumor therapy, PLoS One 11 (3) (2016) e0149482, https://doi.org/10.1371/journal.pone.0149482.
[19] J. Li, et al., Design of an integrated master-slave robotic system for minimally invasive surgery, Int J Med Robot 8 (1) (2012) 77–84, https://doi.org/10.1002/rcs.439.
[20] A.A. Levin, et al., The comparison of the process of manual and robotic positioning of the electrode performing radiofrequency ablation under the control of a surgical navigation system, Sci. Rep. 10 (1) (2020) 8612, https://doi.org/10.1038/s41598-020-64472-9.
[21] H. Lee, et al., A master manipulator with a remote-center-of-motion kinematic structure for a minimally invasive robotic surgical system, Int J Med Robot 14 (1) (2018), https://doi.org/10.1002/rcs.1865.
[22] T. Komaki, et al., Robotic CT-guided out-of-plane needle insertion: comparison of angle accuracy with manual insertion in phantom and measurement of distance accuracy in animals, Eur. Radiol. 30 (3) (2020) 1342–1349, https://doi.org/10.1007/s00330-019-06477-1.